This article has been accepted for publication in a future issue of this journal, but has not been fully edited. Content may change prior to final publication. Citation information: DOI 10.1109/TBME.2017.2777143, IEEE Transactions on Biomedical Engineering

Skull modeling effects in conductivity estimates using parametric electrical impedance tomography

Mariano Fernández-Corazza*, Sergei Turovets, Phan Luu, Nick Price, Carlos Muravchik, *Sr., Member, IEEE*, and Don Tucker

***Abstract*— *Objective:* To estimate scalp, skull, compact bone and marrow bone electrical conductivity values based on Electrical Impedance Tomography (EIT) measurements, and to determine the influence of skull modeling details on the estimates. *Methods:* We collected EIT data with 62 current injection pairs and built five 6-8 million finite element (FE) head models with different grades of skull simplifications for four subjects, including three whose head models serve as Atlas in the scientific literature and in commercial equipment (Colin27 and EGI's Geosource atlases). We estimated electrical conductivity of the scalp, skull, marrow bone and compact bone tissues for each current injection pair, each model, and each subject. *Results:* closure of skull holes in FE models, use of simplified four-layer Boundary Element Method-like models, and neglection the CSF layer produce an overestimation of the skull conductivity of 10%, 10-20%, and 20-30%, respectively (accumulated overestimation of 50-70%). The average extracted conductivities are: 288±53 (the scalp), 4.3±0.08 (the compact bone), and 5.5±1.25 (the whole skull) mS/m. The marrow bone estimates showed large dispersion. *Conclusion:* Present EIT estimates for the skull conductivity are lower than typical literature reference values, but previous *in-vivo* EIT results are likely overestimated due to the use of simpler models. *Significance:* Typical literature values of 7-10mS/m for skull conductivity should be replaced by the present estimated values when using detailed skull head models. We also provide subject specific conductivity estimates for widely used Atlas head models.**

***Index Terms*—Electrical Impedance Tomography, skull electrical conductivity, bioimpedance, biomedical signal processing, electroencephalography.**

I. Introduction

NEURO-DIAGNOSTIC or therapeutic technologies such as Electroencephalography (EEG), Transcranial Electrical Stimulation (TES) and Electrical Impedance Tomography (EIT) require accurate electrical models of the human head. For example, electrical head models are used to estimate cortical sources of scalp recorded signals [1]–[4]. Accurate source estimates are critically important when evaluating patients with refractory epilepsy (i.e., epilepsy not adequately controlled by medication) for surgical resection [5]. Source estimation of EEG signals is also essential for the advancement of basic understanding of cognition and brain functions [6]. In TES, accurate head models are needed to determine optimal current injection patterns and to estimate the electric current density dose delivered to regions of interest in the brain [7]–[10]. TES is actively studied as an emerging therapeutic tool for treatment of depression [11], epilepsy [12], and other neurological disorders [13]. Electrical head models are also important in EIT applications for detection of intracranial bleeding or ischemia in stroke or traumatic brain injury [14], [15].

Anatomically accurate electrical head models are based on segmentation of Magnetic Resonance (MR) and/or Computed Tomography (CT) images into different tissues with specific electrical properties. Initially, simplified three layered spherical models [16] were used, but technological advances have enabled progressively more realistic models that employ anatomically realistic three or four nested layers [17], models that include marrow bone (MB) [18], small foramina in the skull [10], [19], and even blood vessels [20]. The quality of these models depends on both accuracy of characterizing numerous head tissues and their electrical properties, including anisotropy.

The skull and its conductivity are key among these tissue properties. The adult skull is highly resistive compared to the surrounding tissues, acting as an electrical shield between the scalp and brain. Skull cranial plates are composed of two layers of compact bone and a layer of spongy marrow bone sandwiched in the middle. Their conductivity is dependent on subject demographic characteristics such as age, gender and ethnic origin [21].

While tissue types and boundaries can be derived from various imaging data, such as MRI and CT, non-invasive in-vivo determination of the tissue conductivity parameters is still a challenge. Many approaches have been proposed including: magnetoacustic imaging [22], MR-EIT or current density imaging [23]–[25], MR based electrical properties tomography [26], and simultaneous tissue conductivity determination and source localization [27]–[29]. In this paper we are focused on the EIT methods [30], which are portable and most affordable as they are compatible with EEG and can

This work was supported by the ANPCyT PICT2014-1232, UNLP I-209, CONICET, and CICpBA. ST was supported in part by the National Institute of Mental Health (Grant R44MH106421).

MFC* and CHM are with LEICI-Instituto de Investigaciones en Electrónica, Control y Procesamiento de Señales, Universidad Nacional de La Plata (UNLP), CONICET, La Plata, Argentina (correspondence e-mail: marianof.corazza@ing.unlp.edu.ar). MFC*, ST, PL and DT are with the Neuroinformatics Center, University of Oregon, Eugene, OR, US. ST, PL and DT are also with Philips EGI, Eugene, OR, US. PL and DT are with the Department of Psychology, University of Oregon, Eugene, OR, US. CHM is also with Comisión de Investigaciones Científicas, Provincia de Buenos Aires (CICpBA), Argentina.

This article has been accepted for publication in a future issue of this journal, but has not been fully edited. Content may change prior to final publication. Citation information: DOI 10.1109/TBME.2017.2777143, IEEE Transactions on Biomedical Engineering

be implemented within the same EEG system and electrodes.

In medical EIT, harmless electric currents are applied on the subject skin and the resulting electric potentials are recorded with an electrode array [31]. From these boundary voltage measurements, it is possible to reconstruct the internal volumetric conductivity distribution, either voxel-to-voxel basis (imaging EIT, [32]), or just a subset of the regional tissue parameters (parametric or bounded EIT [16], [33]–[35]). An advantage of the bounded EIT (bEIT) approach is that it is able to characterize the conductivity of the most resistive (i.e., the skull) that is invisible to MRI Diffusion Tensor Imaging (DTI) [36]. The typical use of bEIT is to estimate the conductivity values of the upper layers: the scalp and skull [35]. CSF conductivity is well characterized from semi-invasive spinal taps [37]. Brain tissue conductivity estimates from bEIT have a large dispersion. In bEIT, the unknown parameters are varied or adjusted to minimize the difference between the measurements and the model predictions. The computation of the scalp potentials is governed by the Poisson equation and it is known as the EIT forward problem (FP). For spherical models, it can be solved analytically [16], [38]–[43]. For more complex head models, it needs to be formulated and solved numerically by either the Boundary Element Method (BEM) [17], the Finite Element Method (FEM) [35], or the Finite Difference Method (FDM) [44]. In FEM and FDM it is possible to include the inhomogeneous and anisotropic properties of the tissues. On the contrary, BEM models are typically composed by nested and closed surfaces that delimit different homogeneous and isotropic tissue layers. The process of fitting the bEIT data and the simulations is a nonlinear optimization problem, known as the bEIT inverse problem (IP). The methods for solving the IP include Newton's method [35], simplex search [16], [45], least squares through a linearization [46] and simulated annealing [47], [48], among others.

The combination of state-of-the-art electrical head models and bEIT has become a gold standard technique to estimate subject specific scalp and skull conductivity values in-vivo, using simple EEG-like equipment. Previous studies have employed bEIT with different resolution head models and numerical solvers. In one of the earliest studies, Burger and van Milaan used a four terminal scheme with two current injection and two measuring electrodes on the forehead and two analytical models: a uniform sphere and one outer conductive shell model with perfectly insulating skull [49]. They estimated the scalp conductivity value in both models, by varying inter-electrodes distance and using the intersection point of estimates for close electrodes, to be 0.42 S/m, and concluded that at close distances both models reflect reality as all current is shunted through the scalp. Later, Rush & Driscoll conducted an experiment that immersed a postmortem skull in electrolytic fluid and fitted the measurement with a three-layer spherical model [38]. They found good agreement between the experiment and the theory using a skull to scalp conductivity ratio of 1:80.

The bEIT approach continues to be employed in more recent research. Eriksen conducted a typical in-vivo bEIT experiment using 4 subjects, 20 measuring electrodes, one current injection pair, and several frequencies. The best fit for the data in a three-layer spherical model produced an average of 4 mS/m for the skull and 0.53S/m for the scalp conductivities [33]. De Munck et al. proved the stability of the bEIT problem (in contrast with the ill-posed imaging EIT method) through simulations [50]. Ferree et al. proposed a simplex search algorithm for the bEIT inverse problem and a four-layer spherical model as a forward model, and concluded that adding a cerebrospinal fluid (CSF) is important for EEG analysis and for parametric EIT [16]. In the same year, Oostendorp et al. performed another bEIT estimation in-vivo with two subjects, using two injection pairs (AFz-POz and TP7-TP8 in the standard 10-20 EEG montage). They reported a much larger skull conductivity value (13 mS/m) and a lower scalp conductivity value (0.20S/m, the ratio 1:15). It is important to note that these researchers used a three layer BEM head model with a realistic MRI-based geometry but without capturing the skull holes and CSF layer [51]. Gonçalves et al. performed parametric EIT estimations using three-layer BEM models and seven to ten injection pairs. They found average conductivities of 8 mS/m for the skull and 0.33 S/m for the scalp conductivities (ratio 1:40) [17]. Ratio values between 1:15 and 1:40 (instead of the ratio 1:80 initially suggested by Rush and Driscoll) have been widely used in literature since then.

The same range of the scalp to brain conductivity ratio was confirmed in more recent bEIT experiments by He et al. and Clerc et al. [52]–[54]. Clerc et al. used a realistic three-layer BEM model and estimated one parameter at a time assuming a scalp conductivity of 1S/m. They found a scalp/skull ratio of 1:25 that, if we consider a typical scalp conductivity of 0.33 S/m, translates to a skull conductivity value of 0.012 S/m [54]. Zhang et al. estimated the skull conductivity for pediatric subjects *in vivo* and found a value of 16mS/m [55]. This larger value is expected as a pediatric skull is more conductive than an adult skull.

More recently, Dabek et al. used three-layer subject specific BEM models and found skull conductivity to be in the 6.6-7.2 mS/m range and a scalp conductivity of 0.34S/m when averaging the results of 9 subjects [30]. Ouypornkochagorn et al. found a skull conductivity value of 8.4mS/m and a scalp conductivity of 0.58S/m for one subject using a finite element head model of five nested layers (BEM-like model) [56].

In summary, a wide range of skull (from 4 to 20 mS/m) and scalp (from 0.3 to 0.5 S/m, although this is based on a lower number of studies [21]) conductivity values have been reported using bEIT and other methods [21], [52], [57], [58]. These variable estimates might be due to inherent inter-subject and intra-subject variabilities [59], but differences in models used in these studies must be carefully considered.

One of the aims of this paper is to check the hypothesis that the widely-used range of 8-10mS/m for the skull conductivity is significantly overestimated due to neglecting the CSF layer and/or assuming simplified skull models in the processing of experimental bEIT data. Layered BEM-like skull models usually assume a closed skull (with no holes), do not consider

This article has been accepted for publication in a future issue of this journal, but has not been fully edited. Content may change prior to final publication. Citation information: DOI 10.1109/TBME.2017.2777143, IEEE Transactions on Biomedical Engineering

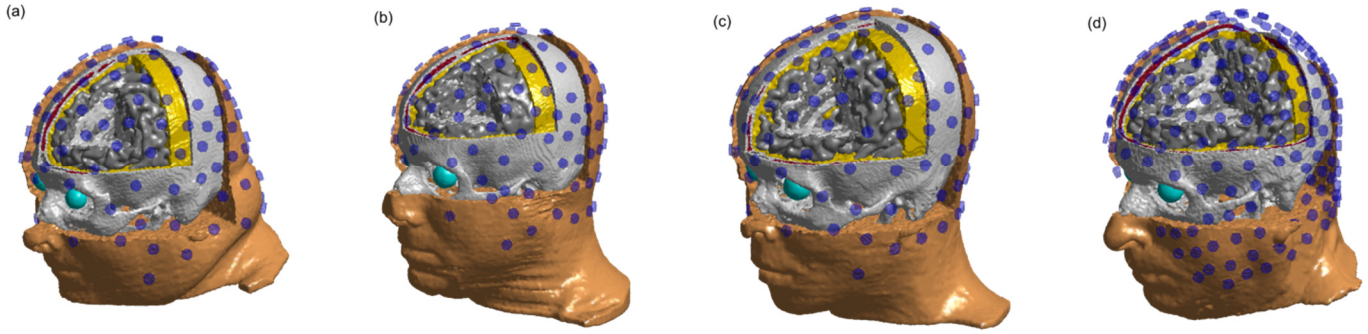

Fig 1: Tetrahedral meshes for four subjects: (a) Atlas Man, (b) Caucasian Atlas, (c) Asian Atlas, and (d) Subject 256. In all cases, the marrow bone is depicted in burgundy color and the electrodes in semi-transparent blue. If carefully observed, it is possible to distinguish the gray-white matter interface and some skull air pockets. Note that Subject 256 has 256 electrodes and no sutures.

the internal air pockets (sinuses), and simplify the rather complex ventral part of the skull geometry. Additionally, regional skull variations may produce inaccurate estimates in studies that used a low number of current injection pairs. While the impact of the skull modeling details on EEG source localization was extensively studied in the past for instance by Lanfer et al. 2012 [4] or Montes-Restrepo et al. 2014 [19], the similar investigation in respect of EIT and specifically parametric EIT has been never undertaken to the best of our knowledge.

In the present work, we estimate scalp and skull conductivities *in-vivo* for four subjects using highly detailed skull models that include major skull openings, minor foramina, realistic skull thickness, internal air and marrow bone. The skull conductivity is estimated in two different ways: assuming it as one homogeneous tissue layer and as a layer split into two different homogeneous tissues (marrow and compact bones). Measurements are obtained using 62 current injection pairs engaging all 128 electrodes covering the whole head, a much larger number than in most of the previous studies. This allows us to obtain a more precise average value. We include a subject wearing a 256-electrode sensor net to improve further intra-subject statistics. To analyze the impact of simplified skull models, we recreated other models from the initial high quality (HQ) ground truth FEM model by closing the skull foramina, by smoothing the skull layer structures (a four-shell BEM-like model), and by replacing the CSF layer by brain tissue (a three-shell BEM-like model). These models allow us to explore the effects of these model assumptions on estimated conductivity values and compare our results with previous literature findings.

Another important aspect of the present work is that we provide scalp and skull conductivity estimates for three subject head models used as atlases in the neuroscience community. One subject is the well-known and widely used Atlas Man (AM) Colin27[1] and two of the subjects are the Caucasian and Asian atlases (CA and AA) used in the EGI source localization package Geosource 3:0[2]. For AM we also estimate the conductivities in the 5-95 Hz frequency range. This work can be considered an extension of our previous conference work where we also showed that different electrode models did not produce a large variation in the conductivity estimates [60]. Thus, we do not analyze different electrode models in the present article.

[1] http://www.bic.mni.mcgill.ca/ServicesAtlases/Colin27
[2] http://www.egi.com

II. Materials and Methods

A. MRI and CT data collection and segmentation

Reference models of soft tissues for the four adult male subjects labelled as AM (Atlas Man), CA (Caucasian Atlas), AA (Asian Atlas) and S256 (a fourth subject wearing a 256-electrode net) aged 44, 46, 52, and 54 years old at the time of scanning respectively were derived from T1-weighted MR images of their heads. Figs. S1 (a) and (b) show the sensor net layouts. The MRI images were obtained with a 3T Allegra scanner (Siemens Healthcare, Erlangen, Germany). The bone structure for AM, CA, and AA was derived from subject-specific CT scans recorded with a GE CT scanner (General Electrics, Fairfield, United States). The acquisition matrix was 256 x 256 x 256 with a voxel size of 1mm x 1mm x 1mm for both the CT and T1 scans. The T1 MRI images were coregistered to the CT space using EGI's segmentation and image processing package, Modal Image Pipeline (BrainK [61]). CT scans for S256 were not available, so Asian atlas (AA) CT scan was warped to the S256 segmentation using a nonlinear warping function in BrainK. T1 MRI images were automatically segmented into six types of tissues (brain gray matter (GM), brain white matter (WM), CSF, scalp, eyeballs, and internal air) using the same package. The skull was segmented from the CT images. Subject bEIT session specific electrode positions for the 128 (for subjects AM, CA, and AA) and 256 (for subject S256) high density EGI sensor nets were determined by using the Geodesic Photogrammetry System (GPS), and coregistered to the CT space with EGI's image software core [62], [63]. Electrodes were added to the segmented volumetric image as 1cm in diameter and 0.7cm in height cylinders of a new tissue corresponding to the conductive gel. The marrow bone segmentation was obtained by combining skull tissue erosion and CT thresholding to preserve compact bone at both the edges and sutures, as studied and recommended in another study [19]. For subject S256, only skull erosion was used as the warped CT was not subject specific.

B. bEIT data Acquisition

All research protocols involving human subjects complied

This article has been accepted for publication in a future issue of this journal, but has not been fully edited. Content may change prior to final publication. Citation information: DOI 10.1109/TBME.2017.2777143, IEEE Transactions on Biomedical Engineering

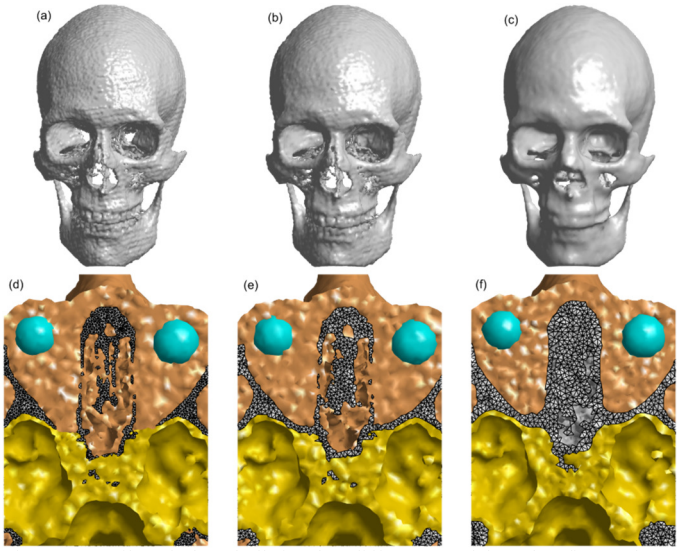

Fig. 2: Details of the skull in the different models. The first column corresponds to the HQ models, the second to the closed-skull model, and the third one to the BEM-like models. The anterior half of the skull is shown in the first row. The eye foramina are open in the first model but closed in the other two models. The BEM-like model (c) is much simpler and smooth. In the second row, we show an axial slice at the height of the eye openings, showing the skull (gray), the scalp (orange), the eyeballs (cyan), and the CSF (yellow). Note that in the BEM-like models the skull is thicker and some details are lost such as the soft tissue inside the nasopharyngeal cavity.

with the ethical standards in the Helsinki Declaration of 1975 and approved by EGI's Institutional Review Boards (IRB). Informed consent was obtained for each subject.

All subjects were fitted with the geodesic sensor net (GSN) and each electrode made contact with the scalp via a conductive gel[3]. Typical EGI electrode contact impedance was around 50 kΩ [64], and the diameter of the contact area is 10mm.

Subjects were positioned in a comfortable chair, and 20μA sinusoidal current at a frequency of 27 Hz was administered for 3 seconds in each of the electrode pairs using one of the automatic software protocols running the EGI 256-channel NA 300 EEG system [34], [65]. For subject AM, the frequency was varied in the 5-95Hz range for two specific pairs (15-72 and 190-46).

For the three subjects wearing the 128 channel GSN, the protocol used 62 current injection pairs, whereas for the subject wearing a 256 channel GSN, the protocol used 130 pairs. Electrode pairs were selected based on electrode distance (for probing deep tissues) and coverage of as much of the head as possible. Table S1 (provided as a separate file) shows the specific pairs used in the 128 and 256-sensor net protocols. Electrode Cz was used as reference for all potential measurements and the sampling rate was 1000 Hz.

From the recorded raw potentials on the scalp, the amplitude of the sinusoids was extracted in a postprocessing step using a software implementation of lock-in detection, with the number of epochs (i.e., the number of the sliding windows in time where the amplitudes were estimated) being $S = 10$ [66]. Due to the low frequency of the injected current, we observed negligible (less than 1 degree) phase shifts between electrode potentials (except for expected change of signs).

C. Finite Element Models

Finite element (FE) tetrahedral meshes of 6 to 8 million of elements were built from the segmented volumetric images using the *iso2mesh* package [67]. This number of elements resulted in a highly detailed virtual model while still being computationally tractable in MATLAB running at the ACISS supercomputing cluster of the University of Oregon[4]. Elements corresponding to internal air pockets were removed and finer meshes were assigned to electrode conductive gel, marrow bone, compact bone, and scalp tissues. The quality of the meshes was assessed by computing the stretch factor, resulting in only <0.1% of the elements of the meshes with an stretch factor lower than 0.05 [68].

We constructed five different models (and corresponding FE meshes) for all four subjects using a combination of the CGAL and the TetGen tools, both included within the *iso2mesh* package [69], [70]. Semi-automatic high-quality mesh generation complexity varied from subject to subject. Summarizing all steps, it took around 8 hours per subject, mostly due to the required manual intervention. With CGAL it is possible to generate tetrahedral meshes directly from the volumetric images. Therefore, it was used for more complex tissues such as the skull, scalp, and electrodes. We started from the segmented image (the output of BrainK) and included electrode segmentation. In the volumetric image, the electrodes were built as cylinders following the normal-to-the-scalp direction. For computing normal-to-the-scalp vectors, a provisional triangular mesh of the outer scalp surface was built and strongly smoothed. This step is semi-automatic as manual interventions are needed for some electrodes where the surface is too curved or near the ears. This process, considering manual interventions, took around 3 hours per subject.

TetGen creates meshes from triangular surfaces that do not self-intersect nor intersect with each other. For this reason, it usually fails for very complex surfaces or surfaces with holes. TetGen was was used for internal tissues: CSF, GM and WM. TetGen requires a three-step procedure: extraction of the surfaces from the volumetric image, conditioning of the surfaces to avoid intersections, and the tetrahedral mesh generation from the conditioned surfaces. In the intermediate step, it is possible to slightly smooth the surfaces resulting in a better-quality mesh. The meshing of the internal tissues was also done in a semi-automatic way, as we iterated between the TetGen scripts, the smoothing process of each surface, and visual inspection in the case of intersections. This process took 3 to 5 hours per subject.

The five models built for each of the 4 subjects were:

[3] http://www.parkerlabs.com/spectra-360.asp

[4] https://aciss-computing.uoregon.edu/

This article has been accepted for publication in a future issue of this journal, but has not been fully edited. Content may change prior to final publication. Citation information: DOI 10.1109/TBME.2017.2777143, IEEE Transactions on Biomedical Engineering

TABLE I
MEANS AND STANDARD DEVIATIONS OF THE CONDUCTIVITY ESTIMATES IN MS/M.

Current injection at 27Hz. σ_{sc}: scalp conductivity, σ_{sk}: skull conductivity (considering the skull as one tissue), σ_{cb}: compact bone conductivity, σ_{mb}: marrow bone conductivity. AM: atlas man, CA: Caucasian atlas, AA: Asian atlas, and S256: subject wearing a 256-electrode net.

Subjects	σ_{sc}	σ_{sk}	σ_{cb}	σ_{mb}
AM	249±54	5.62±2.40	4.16±1.43	298±29
CA	291±61	5.08±1.38	4.22±1.43	138±20
AA	362±66	4.16±0.72	4.25±1.44	146±20
S256	250±53	7.15±2.25	4.35±1.33	173±15
Average	*288±53*	*5.50±1.25*	*4.25±0.08*	-

1) High Quality (HQ) model: In this model, CGAL was used to construct the skull (marrow and compact), scalp, eye ball, and electrode meshes. CSF, GM and WM where built using TetGen. The combination of these two methods results in models with smooth GM surfaces and very detailed skull features, including minor foramina and small bones.
2) HQ model without marrow: This represents the previous model where the tetrahedrons corresponding to the compact and marrow tissues are assigned to only one skull tissue.
3) Closed skull models: To address the effects of just covering the skull holes, we created a very similar model to the HQ model but closing the skull holes as follows: in the segmented image, the CSF tissue was slightly dilated (using a two-voxel structuring element) and the intersection of the expanded CSF and scalp was assigned to the skull. This model has a closed skull, but all other geometrical complexities of the skull are preserved.
4) Layered BEM-like models: These models were built using only TetGen, which requires no self-intersecting surfaces. For this purpose, the skull-CSF and the skull-scalp surfaces had to be strongly smoothened.
5) No-CSF model: These models equal BEM-like models except for the CSF layer, which was replaced by brain tissue. With this model, we address the effects of neglecting the CSF layer as it occurs when using three-layer models in bEIT.

Tissue electrical conductivities. We assigned isotropic and homogeneous average conductivity values to each tissue based on typical values obtained from in vivo, ex-vivo and in vitro human and animal studies (in brackets, we specify the study, the temperature, and the frequency): 0.2 S/m for WM (Gabriel et al., 1996, 37ºC, 200Hz [71], [72]), 0.33 S/m for GM (Gabriel et al., 1996, 37ºC, 200Hz [71], [72]), 1.79 S/m for CSF (Baumann et al., 37ºC, 10Hz [37]), 1.5 S/m for eye balls (Lindenblatt and Silny, 32ºC, 60Hz [73]), and 1.5S/m for gel conductivity at room temperature as measured in [74]. In Fig.1 we show tetrahedral meshes, segmentation, and electrode positions for the HQ-models of the four subjects. In Fig. 2, we depict the major differences between the models for subject AM.

D. Forward Problem:

Volume conduction in the low frequency range of EIT is governed by the quasi-static approximation of Maxwell equations, the Poisson equation [40], [75]. The electrical forward problem (FP) in EIT can be stated as follows: given the electrical head model and a current injection pair, compute the electrical potential at the measuring electrodes. At the top of each gel layer, we imposed the complete electrode model (CEM) boundary conditions [76]. Mathematically, the EIT FP with the CEM conditions is stated as follows:

$$\begin{cases} \vec{\nabla}\left(\boldsymbol{\sigma}\vec{\nabla}\psi\right) = 0 & \text{in } \Omega \\ \boldsymbol{\sigma}\left(\vec{\nabla}\psi\right)\cdot\hat{n} = 0 & \text{in } \delta\Omega \\ \psi + z_l\boldsymbol{\sigma}\left(\vec{\nabla}\psi\right) = V_l & \text{in } \mathrm{E_l} \\ \int_{E_l}\boldsymbol{\sigma}\left(\vec{\nabla}\psi\right)\cdot\hat{n}\ dS = I_l & \text{in } \mathrm{E_l}, \end{cases} \quad (1)$$

where $\boldsymbol{\sigma}$ is the conductivity tensor, ψ is the electric potential, Ω is the solid and $\delta\Omega$ is its boundary, $\hat{n}$ is the normal to the boundary vector, I_l is the injected current at electrode E_l, V_l is the electric potential at electrode E_l, and z_l is the electrode E_l contact impedance.

We solved the Poisson equation with the CEM boundary conditions of (1) numerically, using the first order Finite Element Method (FEM) with the Galerkin approach [77], [78]. In this approach, the FP is reduced to a linear system of equations $\mathbf{Kv} = \mathbf{f}$, where $\mathbf{K}$ is the $(N+L)\times(N+L)$ 'stiffness' matrix, N is the number of mesh nodes and L is the number of electrodes, $\mathbf{v}$ is the unknown $(N+L)\times 1$ vector of the electric potential at each node, and $\mathbf{f}$ is a $(N+L)\times 1$ vector with the current injection information. The $\mathbf{K}$ matrix considers the geometry and conductivity of each tissue and the CEM contact impedances. $\mathbf{K}$ is built in a completely automatic way using our own FEM MATLAB scripts with parallel computing (taking approximately 10 minutes on a node of the ACISS cluster with 12 cores and 72GB of RAM). Detailed information about $\mathbf{K}$ and $\mathbf{f}$ formulations can be found elsewhere [35], [76].

A preconditioned conjugated gradient (PCG) algorithm in MATLAB was used to solve the resulting linear system $\mathbf{Kv} = \mathbf{f}$ with the LU factorization matrices as preconditioners [79]. Typical solutions for 6 million element models required approximately 200 PCG iterations and 1 minute of computation time with a tolerance of 1×10^{-11} for the residuals.

For every model, if assuming homogeneous and isotropic conductivity values for each tissue, dependencies of the stiffness matrix on tissue conductivities can be stated as follows:

$$\mathbf{K}(\boldsymbol{\theta})\mathbf{v} = \left(\sum_{i=1}^{B}\sigma_i\mathbf{K}_i\right)\mathbf{v} = \mathbf{f}, \quad (2)$$

where $\boldsymbol{\theta}$ is the vector of unknown conductivity values σ_i, $\mathbf{K_i}$ are the stiffness matrices for each tissue i, and B is the number of tissues. Details of deriving (2) from the FEM formulation is shown in previous work [35].

E. Inverse problem:

This article has been accepted for publication in a future issue of this journal, but has not been fully edited. Content may change prior to final publication. Citation information: DOI 10.1109/TBME.2017.2777143, IEEE Transactions on Biomedical Engineering

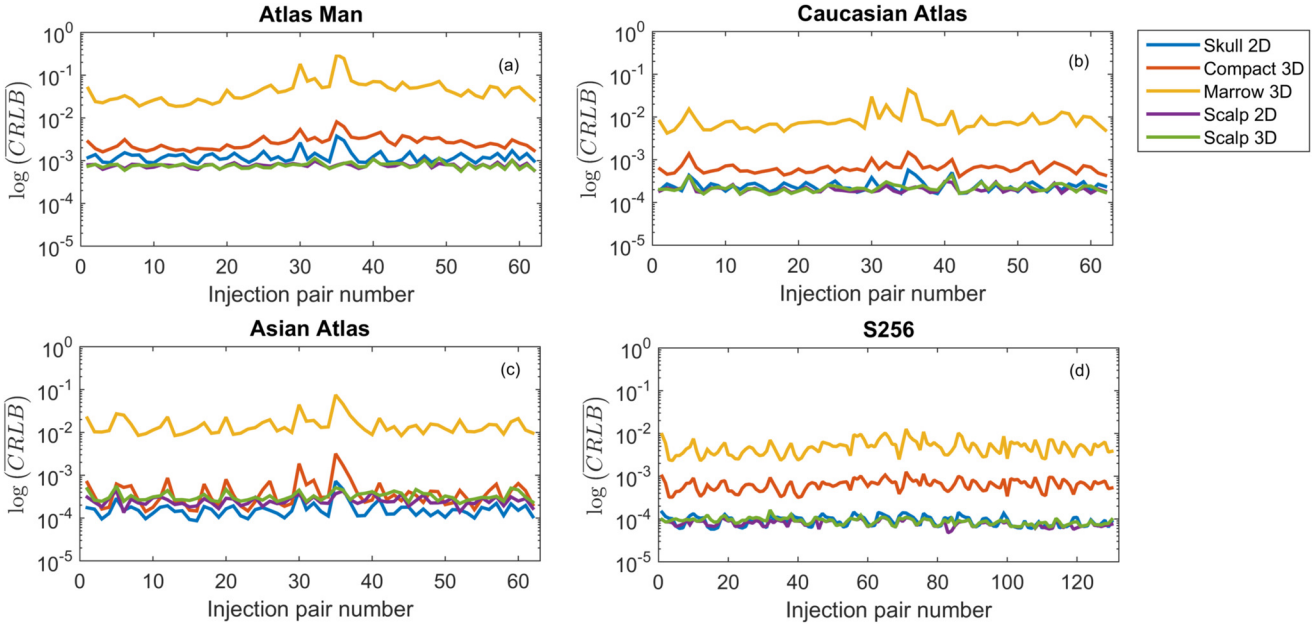

Fig 3: Normalized CRLB for the estimates in the 2-parameter and 3-parameter searches, and for all four subjects. Note that the normalized CRLB corresponding to the marrow bone is the largest, one or two orders of magnitude larger than the normalized CRLB of the other tissues.

The EIT Inverse Problem (IP) involves estimation of model parameters (typically, the electrical conductivity values) from the electric potential measurements. The least squares approach minimizes the ℓ_2-norm of the difference between the model predictions and the actual measurements:

$$\widehat{\boldsymbol{\theta}} = \underset{\boldsymbol{\theta}}{\operatorname{argmin}}\{(\bar{\mathbf{y}} - \mathbf{M}\mathbf{K}^{-1}(\boldsymbol{\theta})\mathbf{f})^T(\bar{\mathbf{y}} - \mathbf{M}\mathbf{K}^{-1}(\boldsymbol{\theta})\mathbf{f})\}, \quad (3)$$

Where $\boldsymbol{\theta}$ is the parameter vector, $\mathbf{M}$ is an $(L-1)\times(N+L)$ sparse selection matrix that selects the last L elements of $\mathbf{v}$, and the $(L-1)\times 1$ vector $\bar{\mathbf{y}}$ is the average of S samples. Each sample is an output of the lock-in detector.

It can be shown that $\widehat{\boldsymbol{\theta}}$ is the Maximum Likelihood Estimator under a Gaussian measurement model [35], [80]. In a noiseless scenario, the problem of (3) is convex and ill-conditioned, meaning that there is only one global minimum in a "valley" that is almost flat in one direction and very sharp in another, making it difficult to solve (see Fig. 6 of [81], or Fig. 1E of [82]).

Several numerical optimization methods can be used to solve (3). We use the classic Newton's method that requires the partial derivatives of $\mathbf{M}\mathbf{K}^{-1}(\boldsymbol{\theta})\mathbf{f}$ with respect to each unknown parameter θ_i to compute the Gradient vector and the Hessian matrix. Using matrix calculus, these derivatives are easily found for the FEM expressions as:

$$\begin{aligned}\frac{\partial \mathbf{M}\mathbf{K}^{-1}(\boldsymbol{\theta})\mathbf{f}}{\partial\theta_i} &= \mathbf{M}\left(-\mathbf{K}^{-1}(\boldsymbol{\theta})\frac{\partial \mathbf{K}(\boldsymbol{\theta})}{\partial\theta_i}\mathbf{K}^{-1}(\boldsymbol{\theta})\right)\mathbf{f} \\ &= -\mathbf{M}\mathbf{K}^{-1}(\boldsymbol{\theta})\frac{\partial \mathbf{K}(\boldsymbol{\theta})}{\partial\theta_i}\mathbf{u}.\end{aligned} \quad (4)$$

From (2), it can be easily shown that:

$$\frac{\partial \mathbf{K}(\boldsymbol{\theta})}{\partial\theta_i} = \mathbf{K}_i, \quad (5)$$

i.e., the stiffness matrix of tissue i. Newton's method requires a smaller number of iterations than other numerical optimization methods. Moreover, we empirically found that it was more stable for this problem than the Nelder-Mead simplex search method [83], and that the method stagnated after six to eight iterations (see Fig. S2). We set the method to stop after nine iterations, with examples from simulated and real data shown in supplementary Fig. S2. The numerical stability and speed of convergence was better for initial values lower than the reference conductivities, as the cost function landscape is steepest at low values of the conductivities (see Fig. 6 of [81], or Fig. 1E of [82]). Specifically, we chose 0.2S/m for the scalp and 1mS/m for the skull and the compact bone as initial conductivity values for faster convergence to the global minimum.

F. Cramér-Rao Lower Bound

The Cramér-Rao lower bound (CRLB) is a lower bound of the variance for any unbiased estimator [80]. That is, no estimation algorithm can have a lower covariance matrix than CRLB. In this work, we use CRLB to assess the quality of the estimates (electrical conductivity of the scalp, skull as a whole, compact bone and marrow bone) in a similar manner as in a previous work [35].

If $\widehat{\boldsymbol{\theta}}$ is an unbiased estimator of $\boldsymbol{\theta}$, then its covariance matrix satisfies: $Cov\{\widehat{\boldsymbol{\theta}}\} \geq CRLB(\boldsymbol{\theta}) = J^{-1}(\boldsymbol{\theta})$, where the matrix inequality implies that the difference is positive semidefinite, J is the Fisher information matrix, and Cov stands for covariance. For signals with white Gaussian noise, J is given by

$$[J(\boldsymbol{\theta})]_{ij} = \frac{S}{v_w^2}\left(\frac{\partial \boldsymbol{\mu}(\boldsymbol{\theta})}{\partial\theta_i}\right)^T\left(\frac{\partial \boldsymbol{\mu}(\boldsymbol{\theta})}{\partial\theta_j}\right), \quad (6)$$

where $\boldsymbol{\mu}(\boldsymbol{\theta}) = \mathbf{M}\mathbf{K}^{-1}(\boldsymbol{\theta})\mathbf{f}$ is the expected value of the measurements, S is the total number of samples, and v_w is the noise standard deviation [80]. Partial derivatives of (6) were shown in (4).

To account for the different order of magnitude of the parameters, we define a normalized CRLB for each parameter θ_i as:

This article has been accepted for publication in a future issue of this journal, but has not been fully edited. Content may change prior to final publication. Citation information: DOI 10.1109/TBME.2017.2777143, IEEE Transactions on Biomedical Engineering

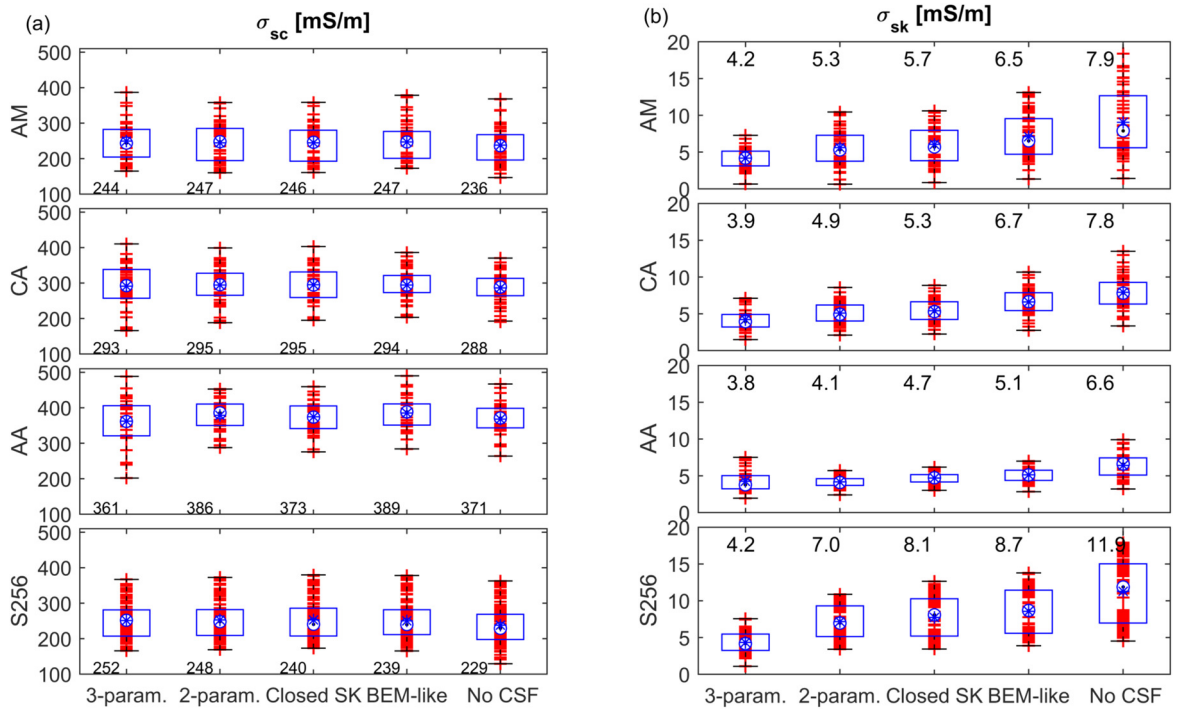

Fig. 4: Box plots of the estimates using real data for the scalp (a) and skull (b) conductivity values using the 5 different models and for the four subjects. Each red cross represents the estimate for one current injection pair, circle indicates the median (which is also given in numbers), blue asterisk represents the mean, and edges of the blue box are the 25th and 75th percentiles. The first box plot in each graph of (b) corresponds to the compact bone conductivity of the 3-parameter search while the other values correspond to conductivity estimates of the skull as a whole. It is clearly seen that the mean skull conductivity estimates are larger when the model is simpler, but the scalp conductivity estimates remain almost unaltered.

$$\overline{CRLB_i} = \frac{\sqrt{CRLB_{ii}}}{\theta_i}, \qquad (7)$$

where θ_i is a reference value for each parameter, and $CRLB_{ii}$ is the *i-th* element of the diagonal of the CRLB matrix. This coefficient is equivalent to a bound on the relative standard deviation of each parameter and it was defined as the Coefficient of Variation Bound (CVB) in our previous work [35].

III. Results

For all subjects and for each current injection pair we estimated the scalp, compact bone, and marrow bone conductivities (a 3-parameter search) and also the scalp and skull conductivities assuming compact and marrow bone as only one tissue (a 2-parameter search). Some current injection pairs were excluded from the analysis because either the inverse search didn't converge after nine iterations or the estimates were unrealistic (marked as outliers). Table I shows the mean and dispersion among the different current injection pairs of the 2-parameter and 3-parameter estimates. The standard deviations of the first four rows correspond to the variability among the estimates obtained with the different current injection pairs whereas the standard deviations of the last row correspond to the variability of the mean of the four subject estimates. Note the large relative dispersion of the marrow bone estimation.

Two-sample t-tests were performed to statistically evaluate the estimates between the four subjects. All six comparisons of the compact bone estimates failed to reach statistical significance ($p \geq 0.47$). For the skull (in 2D search) and scalp estimates, test results showed statistically different in almost all cases, $p \leq 0.05$ (except for the scalp conductivity between AM and S256, $p = 0.85$, and for the skull conductivity between AM and CA, $p = 0.14$).

For comparison of the quality of the marrow bone estimates with the quality of the other tissue estimates, Fig. 3 presents normalized Cramér-Rao lower bound for the four subjects. It is observed that the variance bound of the marrow bone estimates is theoretically one or two orders of magnitude larger than the estimates of the other tissues. In (6) we used the number of samples of the real data, $S = 10$, and derived the noise standard deviation also from real data, $v_w = 0.82\ \mu V$.

To study the impacts of using closed-skull, BEM-like and No-CSF models, we performed the inverse search also for these three models using both synthetic and real data. The synthetic data were simulated using the HQ-model (including marrow bone) with the estimated mean conductivities for scalp and compact bone, but with literature conductivity value for the marrow bone. Fig. 4 shows results based on experimental bEIT data for subjects AM, CA, AA, and S256, and Fig. 5 shows results based on synthetic data. The 3-parameter estimates correspond to the compact bone layer but in all other cases the estimates correspond to the skull as a homogeneous tissue. Note that for all subjects, the more simplified model the model is, the more overestimated the skull conductivity is (and the larger variance of the estimates across different current injection pairs). This is seen for both real and synthetic data.

For each of the five models, four subjects, and - at least - 62 current injection pairs, the conductivity estimation involved 9

This article has been accepted for publication in a future issue of this journal, but has not been fully edited. Content may change prior to final publication. Citation information: DOI 10.1109/TBME.2017.2777143, IEEE Transactions on Biomedical Engineering

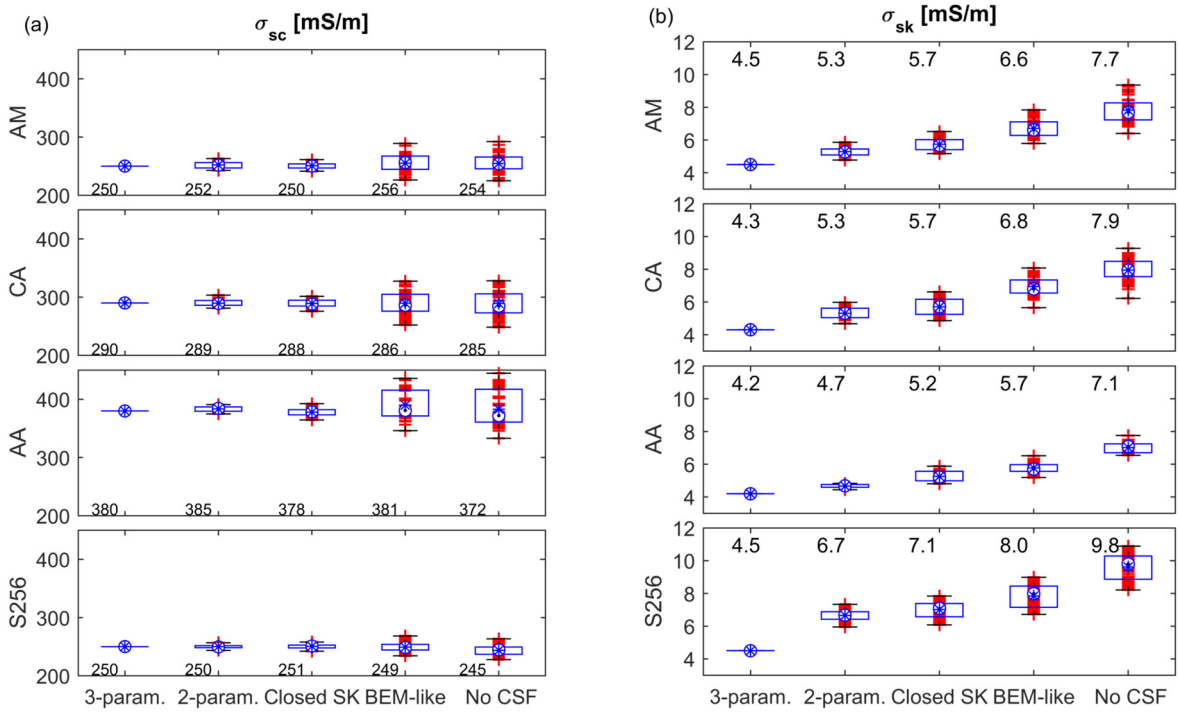

Fig. 5: Box plots of the estimates using synthetic data for the scalp (a) and skull (b) conductivity values using the 5 different models and for the four subjects. Each red cross represents the estimate for one current injection pair, circle indicates the median (which is also given in numbers), blue asterisk represents the mean, and edges of the blue box are the 25th and 75th percentiles. The first box plot in each graph of (b) corresponds to the compact bone conductivity of the 3-parameter search while the other values correspond to conductivity estimates of the skull as a whole. As in this figure we show the estimates obtained from the synthetic signals, this first box in each graph acts as a validation of the estimation method. It is clearly seen that the skull conductivity estimates are larger when the model is simpler, but the scalp conductivity estimates remain almost unaltered, as when using real data.

iterations of the Newton's method requiring 7 (for 2-parameters) or 15 (for 3-parameters) forward problem computations (Gradient and Hessian) of approximately one minute each. This huge computational load ran at the University of Oregon ACISS supercomputing cluster using parallel MATLAB programming.

We also conducted experiments for AM subject with one injection pair varying the injected current frequency. In Fig. 6, the estimates of the skull conductivity with respect to the frequency are shown. It can be seen that there is a slight increase in conductivity as a function of frequency, in line with in-vitro measurements by Akhtari et al. [84]. Superimposed on the estimates is the adjusted Akhtari's function ($\sigma[mS/m] = A\omega^{\alpha}$, where ω is 2π times the frequency) for the 2-parameter skull conductivity estimates and for the 3-parameter compact bone conductivity estimates, with the best fits for A values (3.35 for 2D and 3.93 for 3D searches) and α values (0.032 for 2D and 0.024 for 3D).

To give an example of the modeling accuracy impact on dose calculations in TES, a simple simulation targeting cortical area M1 in AM was performed. The ground truth EEG and TES lead fields within the HQ model was simulated, and the dose (current density) at the region of interest with the simplified versions of the skull and the corresponding bEIT estimates for the same amplitude of TES current of 1 mA was computed. The reciprocity principle was used as the targeting strategy, with 1 source and 5 sinks in an opposite configuration [10]. The averaged current densities at the cortex ROI were 0.1516, 0.1535, 0.1582, 0.1639, and 0.0957 A/m^2 for the HQ, HQ without marrow, closed skull, BEM-like, and no-CSF models, respectively. Fig. 7 shows the module of the current density on the cortex for four head models.

IV. Discussion

In this paper, we extended our previous results by adding the scalp and skull conductivity estimates for a larger pool of subjects (atlases), by including the marrow and compact bone estimates and the closed-skull model, and by adding more elements to the FE meshes improving its quality [35], [60].

A. New estimates, including atlases.

We provide new scalp, skull, and compact bone conductivity estimates shown in Table I for four subjects, three of them being atlases widely used in the EEG community. Note that subject CA and S256 are partially bald, so smaller scalp conductivities are expected due to the skin exposure to air. At the same time, the skull conductivities for these subjects are somewhat larger than the skull conductivity of AA. This was expected as CA skull is thicker than the skull of AA. The values of the new estimates for the scalp are close to the literature values, but lower for the skull conductivities.

The tissue conductivity data of three of the four subjects of this study are important because they are widely used as atlases in EEG source localization, for instance the CA and AA based ones in Geosource 3:0 [85], [86], and the AM based BEM in LORETA [87], EEGLAB-NFT [88], Brainstorm [89], and FieldTrip [90]; and as an FEM in COMETS [91] and BrainStimulator software released with the SCIRun package [92].

This article has been accepted for publication in a future issue of this journal, but has not been fully edited. Content may change prior to final publication. Citation information: DOI 10.1109/TBME.2017.2777143, IEEE Transactions on Biomedical Engineering

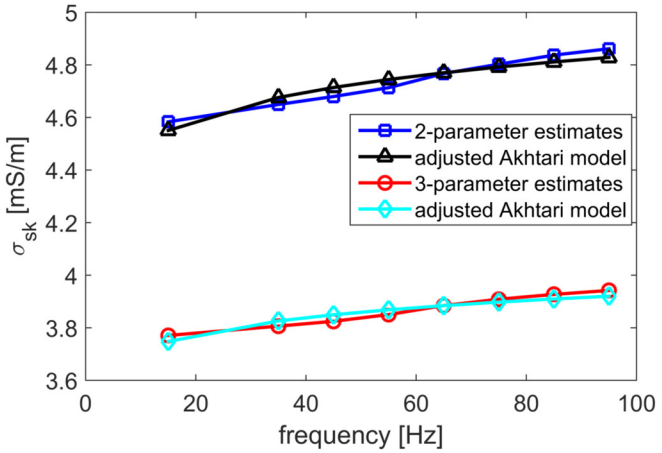

Fig 6: skull conductivity estimates for the 2-parameter search and compact bone conductivity estimates for the 3-parameter search versus the frequency. These results are based on real data for subject AM. The two adjusted Akhtari models are also shown.

A novelty of this work is the estimation of the scalp, compact and marrow conductivities in a 3-parameter search using highly detailed head models. Note that a very accurate segmentation of the raw MRI/CT data is required for building these HQ models that preserve many skull details and realistic ratios between thicknesses of the tissues. In Table I, one can see the low dispersion of the compact bone among the different subjects, and this is a major finding of this work. Note that, due to the marrow bone, the compact bone estimates in the 3-parameter search are 10-20% lower than the skull conductivity estimates assuming it as a homogeneous tissue. Except for S256, where the difference between skull conductivity and compact bone conductivity is around 60%. This is also seen in the simulations. This effect might be explained by the fact that the skull is not "native" for this subject but warped from the atlas.

To our knowledge, we provide the first estimates of the compact bone *in vivo* using parametric EIT. The estimates are in a good agreement with the in-vitro estimates of the live human skull conductivities given by Tang et al. [93], who found a standard compact layer conductivity of 3.7±0.5mS/m averaged over 60 samples, and a quasi-compact conductivity of 5±0.7mS/m averaged over 53 samples, and with the lower estimate of Law [59] for the compact bone (4.7mS/m). Our estimates are also within the range reported by Akhtari et al. [94], 2.8-10.2mS/m, based on four samples. For the skull as a whole, Tang et at reported a conductivity of 12.5mS/m for a perfect three-layer structure, and 7mS/m for a quasi-three layer structure. Ahktari et al. reported a "bulk" conductivity in the 8.5-11.4 mS/m range, and Law reported (based on postmortem samples) a very wide range for different skull samples (4.7-73mS/m).

In-vitro estimates are always "local" while the parametric EIT approach estimates a global average fit. Our parametric EIT estimates for whole skull conductivity value agree well with previous parametric EIT studies [17], [24], [30], when we downgrade our initial detailed models to their simpler BEM-like models.

B. *Influence of the marrow bone*

Due to the ill-conditioned nature of the problem (there is only a small fraction of the marrow bone relative to the head volume and therefore, a low sensitivity of bEIT procedure to marrow bone variations), we found very large variability in the estimates. Indeed, the CRLB for this tissue is one or two orders of magnitude larger than the CRLB of the other tissues, meaning that estimating the marrow bone using bEIT is extremely difficult for any unbiased bEIT estimator. However, the 3-parameter search is still valid to estimate the compact bone conductivity. If the marrow bone is to be estimated for use in electromagnetic modeling applications (EEG, EIT, TES), a large CRLB also indicates a lesser influence on these problems. In practical applications, a very accurate MB conductivity value might not be required.

C. *Skull models*

We showed that the simpler model for the skull is, the larger its conductivity estimates derived from the same experimental bEIT data are, and this is a major finding of this paper. All three simplifications produced significant overestimations. First, closing skull holes resulted in an overestimation of ~10% of skull conductivity. Second, a recreation of the BEM-like models produced an additional overestimation of ~15% (20-35% compared to the HQ model). Finally, neglecting the CSF layer produced an additional ~25% overestimation (50-70% compared to the HQ model). Thus, different skull model simplifications consistently lead to overestimates of the skull conductivity by 10 to 70% across the different subjects, also when using synthetic data.

The present findings can be used to adjust the *in-vivo* bEIT results of prior work that used anatomically approximate BEM-like or three-layer head models. When using these simpler models, we found typical literature values of 7-12 mS/m [30]. As these literature values were mostly estimated using BEM-like models and neglecting the CSF, we showed that these typical values are overestimations of the actual skull conductivity. In Turovets et. al. [34], a factor of 2 was introduced due to a confusion between the peak and peak-to-peak amplitudes of the injection currents, therefore the skull estimates were also overestimated by factor of 2. If corrected by this factor, they agree with the present work.

The new values shown in Table I should be considered as better estimates in future precise head modeling studies. At the same time, within a simple BEM model, the skull conductivity estimate in the range of 7-12 mS/m is a good fit for the bEIT scalp data. Therefore, in terms of "calibration" of these simpler models, the overestimated values might be used in source localization [95], or this calibration could be achieved by using the bEIT approach detailed in this paper.

The skull models can be improved even further, for example by mapping the skull porosity derived from the CT Hounsfield units to electrical conductivity [9]. This mapping is parametric, with a low number of unknowns and bEIT can be used to estimate them in a similar way as shown in the present work.

D. *Frequency response*

This article has been accepted for publication in a future issue of this journal, but has not been fully edited. Content may change prior to final publication. Citation information: DOI 10.1109/TBME.2017.2777143, IEEE Transactions on Biomedical Engineering

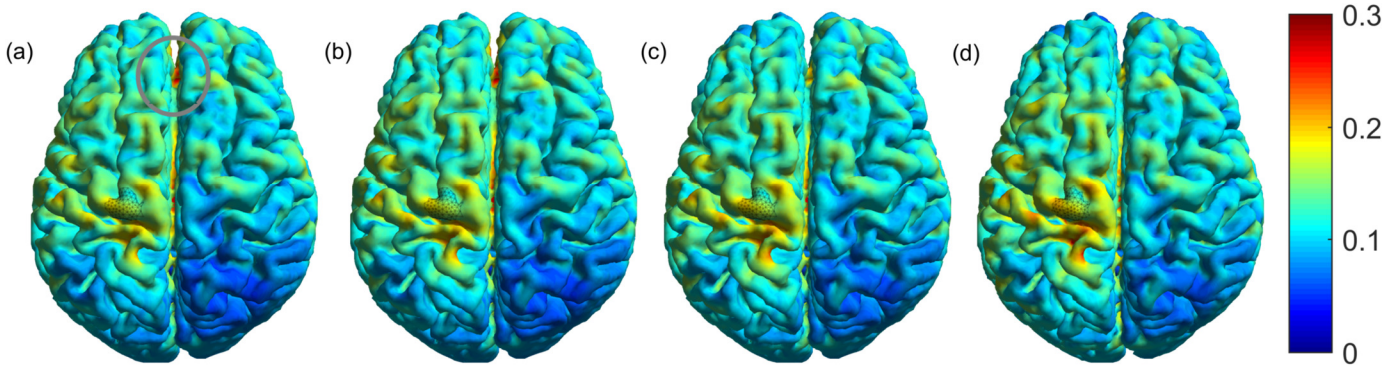

Fig 7. Current density on cortex [A/m2] when stimulating a ROI at the motor cortex using four different models and their specific conductivity estimates: (a) HQ, (b) HQ without marrow, (c) closed skull, and (d) BEM-like models. In the first three models, the differences are almost imperceptible, in the fourth model the computed dose is slightly larger. Note how the "hot spot" at the frontal part of the medial plane (circled in gray) is significantly reduced when patching the skull holes. This also indicates the relevance of using detailed models in TES.

We found that the Akhtari model [84] for the frequency response of the skull conductivity at low frequencies fits to our in-vivo data with "A" and "alpha" parameters in the same reported range. The frequency response variation of our estimates is like the variation reported by Dabek et al. [30], with a skull conductivity variation of around 6% in the 20 to 100 Hz range. We also found the scalp conductivity to be almost constant in this low frequency range (around 1% variation). Note that in the Akhtari model, an "alpha" value lower than 1 is like a squared-root shaped plot. However, as it is shown in Fig. 6, we found conductivity vs frequency relation to be mostly linear or a slightly exponential function, which is more like the plots shown in Dabek et. al [30].

Due to the technical specifications of the EIT equipment used in this work, we focused in the low frequency range (< 100 Hz). However, in some applications such as classical imaging EIT [31] or modeling Tumor Treating fields [96], knowing the background conductivities at higher frequencies (typically in the kHz range) may be important. With a typical EIT equipment in the kHz range, the same pipeline followed in this work can be replicated to get this valuable information.

E. Impacts in EEG and in TES

The impact of different skull models in the EEG source localization problem have been widely studied in the literature [2], [4], [19], [63], [97]–[99]. All these studies emphasize a need for accurate estimates of the different tissue conductivities, particularly the skull, as their miss-specification can lead up to several centimeters error in source localization. In this paper, we presented a framework of parametric EIT to estimate the scalp, skull, and compact bone electrical conductivity values, in-vivo, individually for each subject, that can be implemented as a routine procedure before an EEG or TES study.

In TES, the impact of skull modeling effects and other head tissue conductivities on resulting focality and dosage is also significant (see for example Fig. S1 in [10] and also [100]–[103]). In Fig. 7, we illustrate the skull modelling effects upon a simple example of targeting the motor cortex. We found that when the skull conductivity estimates varied 10-30% among the different models, the actual current intensity variations on the cortical target were lower (up to 8%) for the first four models when using the best estimate for each specific model. The effects of patching the skull holes was found to be less significant (4%) than using a BEM-like model (8%). However, depending on the application, an 8% error in dose might be significant. Another important aspect is what happens at the non-ROI. In Fig. 7, one can observe how the "hot spot" at the frontal part of the medial plane (circled in gray) is significantly reduced when closing the skull holes. This is probably due to closing eye foramina. Thus, although using a simpler model might not produce significant dose miss-estimates at a given ROI, it might significantly miss-estimate "hot spots" at the non-ROI. Note that the ROI (M1) in this example belongs to a brain region where there are no apparent skull holes nearby and where the skull shape is mostly round. The delivered dose when targeting other ROIs closer to any skull foramina or deeper ROIs might be more sensitive to different skull models, even if calibrated using EIT. This example shows the potential relevance of using anatomically faithful models in TES. More detailed studies are required to address the effects of using models of different anatomical complexity, with or without calibration for different ROIs of clinical interest. These studies are beyond the scope of this paper and relegated for future work.

F. Limitations

Although the bEIT methodology to extract the regional conductivity used in this paper was well tested and validated in physical phantoms, for example in [65], [104], there is still work to do in human experiments to provide a direct and accurate reference to compare with.

Due to inter-subject variability, a larger number of subjects would be required to corroborate the reported values and improve the statistical analysis of electrical conductivity of the head tissues. In this sense, a similar study with a pool of 14 subjects is being carried out [82].

The model generation pipeline used in this work involves subject specific MR and CT images. These data are not always available and, if available, the construction of the models might be complex, time consuming, and the segmentation might vary for different segmentation protocols. However, the applicability of the general method is wider, as approximated models can be calibrated using the bEIT method presented in

the paper. A detailed analysis of possible alternatives when subject specific CT and/or MR images are not available (such as using conformal atlas head models warped to an individual subject head shape, or average models), and the accuracy of calibrated models is left for future studies. Also, it is of value to cross-validate the present results with different segmentation software packages, which may produce somewhat different tissue layer thicknesses and therefore somewhat different bEIT estimates even for the same MR, CT, and raw bEIT data.

There are other factors that might contribute to the accuracy of the extracted scalp and skull conductivity values. For example, the assumed conductivity of other intracranial tissues might affect estimates of the scalp and skull conductivity values. However, the CSF conductivity is well known [37], and the sensitivity of the parametric EIT method with respect to the brain conductivity is relatively low [34], [35]. Furthermore, electrode modeling can also affect scalp and skull conductivity estimates, but this has been shown to be relatively minor [60]. The effects of other modeling enhancements such as the inclusion of the dura layer [105] or the major blood vessels [20] should be analyzed in future studies.

V. Conclusions

Bounded or parametric EIT can be used to accurately estimate the scalp, skull and compact bone conductivities, non-invasively and *in-vivo*, and is an excellent approach for dealing with inter-subject variability. The goal of bEIT can be either to estimate the electrical conductivity values of the head tissues *per-se* or to "calibrate" electrical head models to be used in, for example, EEG or TES problems.

In the first case, the more precise the model is, the more accurate the estimates are. We showed that different skull modeling simplifications used in the literature might lead (when combined) to up to 70% of the skull conductivity overestimation in bEIT.

For the second case, if the goal is to calibrate an electrical head model for EEG source localization or TES, bEIT is key for performing the calibration. A simpler model tuned to the conductivities providing the best fit to the scalp bEIT data might produce less significant errors than the same simpler model with the true or literature conductivity data. In the example of targeting the motor cortex we found that a simpler model lead to a miss-estimate of 8% of the delivered dose, when using calibrated EIT estimates. We observed that for some regions next to the skull foramina, the effects of using closed skull models could possibly be larger. Further studies are required to analyze in more detail to what extent the errors produced by simpler models, even if calibrated, are relevant or not.

We found average scalp conductivity of 288 mS/m, compact bone conductivity of 4.3 mS/m, and skull conductivity of 5.5 mS/m. The conductivity estimates of the widely-used Colin27 atlas man head model were 249 mS/m, 4.2mS/m, and 5.6mS/m for the scalp, compact bone, and the entire skull conductivity respectively. The electrical conductivity of the Caucasian and Asian atlases (CA and AA) can be also found in Table I. Extracted scalp and skull conductivities were statistically different among four subjects, proving inter-subject variability. However, the compact bone estimates were statistically similar. To the best of our knowledge, we used the largest number of current injection pairs compared to the other bEIT literature works. Also, this is the only work so far that estimates compact bone conductivity *in-vivo* using EIT.

VI. Acknowledgment

Author MFC acknowledges the Fulbright Foundation, USA, the Fundación Bunge & Born, Argentina, the UNLP, Argentina, and EGI, USA, which supported visits to the University of Oregon Neuroinformatics Center and EGI, Eugene, USA, where most of this work has been done.

Conflicts of interest: Authors ST, PL, and DT are employees of Philips EGI, a manufacturer of dense array EEG and TES systems. MFC and CM, are employees of La Plata University, the CONICET and the CICpBA, Argentina, and have no commercial interest in EGI's products.

References

[1] B. Vanrumste *et al.*, "Dipole location errors in electroencephalogram source analysis due to volume conductor model errors," *Med Biol Eng Comput*, vol. 38, no. 5, pp. 528–534, 2000.

[2] C. H. Wolters, A. Anwander, X. Tricoche, D. Weinstein, M. A. Koch, and R. S. MacLeod, "Influence of tissue conductivity anisotropy on EEG/MEG field and return current computation in a realistic head model: A simulation and visualization study using high-resolution finite element modeling," *Neuroimage*, vol. 30, no. 3, pp. 813–826, Apr. 2006.

[3] R. Grech *et al.*, "Review on solving the inverse problem in EEG source analysis," *J. Neuroeng. Rehabil.*, vol. 5, no. 1, p. 25, 2008.

[4] B. Lanfer, M. Scherg, M. Dannhauer, T. R. Knösche, M. Burger, and C. H. Wolters, "Influences of skull segmentation inaccuracies on EEG source analysis," *Neuroimage*, vol. 62, no. 1, pp. 418–431, 2012.

[5] V. Brodbeck *et al.*, "Electroencephalographic source imaging: a prospective study of 152 operated epileptic patients," *Brain*, vol. 134, no. 10, pp. 2887–2897, Oct. 2011.

[6] L. Spyrou and S. Sanei, "Source Localization of Event-Related Potentials Incorporating Spatial Notch Filters," *IEEE Trans. Biomed. Eng.*, vol. 55, no. 9, pp. 2232–2239, Sep. 2008.

[7] J. P. Dmochowski, M. Bikson, A. Datta, Y. Su, and L. C. Parra, "A multiple electrode scheme for optimal non-invasive electrical stimulation," in *2011 5th International IEEE/EMBS Conference on Neural Engineering*, 2011, pp. 29–35.

[8] A. Opitz, W. Paulus, S. Will, A. Antunes, and A. Thielscher, "Determinants of the electric field during transcranial direct current stimulation," *Neuroimage*, vol. 109, pp. 140–150, 2015.

[9] S. Guler *et al.*, "Optimization of focality and direction in dense electrode array transcranial direct current stimulation (tDCS)," *J. Neural Eng.*, vol. 13, no. 3, pp. 1–14, Jun. 2016.

[10] M. Fernández-Corazza, S. Turovets, P. Luu, E. Anderson, and D. Tucker, "Transcranial Electrical Neuromodulation Based on the Reciprocity Principle," *Front. Psychiatry*, vol. 7, May 2016.

[11] U. G. Kalu, C. E. Sexton, C. K. Loo, and K. P. Ebmeier, "Transcranial direct current stimulation in the treatment of major depression: a meta-analysis," *Psychol. Med.*, vol. 42, no. 9, pp. 1791–1800, Sep. 2012.

[12] S.-W. Yook, S.-H. Park, J.-H. Seo, S.-J. Kim, and M.-H. Ko, "Suppression of Seizure by Cathodal Transcranial Direct Current Stimulation in an Epileptic Patient - A Case Report -," *Ann. Rehabil. Med.*, vol. 35, no. 4, pp. 579–582, 2011.

[13] A. R. Brunoni, F. Fregni, A. Priori, R. Ferrucci, and P. S. Boggio, "Transcranial direct current stimulation: challenges, opportunities and impact on psychiatry and neurorehabilitation," *Front. Psychiatry*, vol. 4, no. 19, 2013.

[14] J. P. J. J. Abascal *et al.*, "Use of anisotropic modelling in electrical impedance tomography; Description of method and preliminary assessment of utility in imaging brain function in the adult human

head," *Neuroimage*, vol. 43, no. 2, pp. 258–268, Nov. 2008.

[15] T. Tang and R. J. Sadleir, "Quantification of intraventricular hemorrhage with electrical impedance tomography using a spherical model," *Physiol. Meas.*, vol. 32, no. 7, pp. 811–821, 2011.

[16] T. C. Ferree, K. J. Eriksen, and D. M. Tucker, "Regional head tissue conductivity estimation for improved EEG analysis.," *IEEE Trans. Biomed. Eng.*, vol. 47, no. 12, pp. 1584–92, Dec. 2000.

[17] S. I. Goncalves, J. C. de Munck, J. P. a. Verbunt, F. Bijma, R. M. Heethaar, and F. Lopes da Silva, "In vivo measurement of the brain and skull resistivities using an eit-based method and realistic models for the head," *IEEE Trans. Biomed. Eng.*, vol. 50, no. 6, pp. 754–767, 2003.

[18] N. von Ellenrieder, L. Beltrachini, C. H. Muravchik, and J. Gotman, "Extent of cortical generators visible on the scalp: Effect of a subdural grid," *Neuroimage*, vol. 101, pp. 787–795, Nov. 2014.

[19] V. Montes-Restrepo, P. van Mierlo, G. Strobbe, S. Staelens, S. Vandenberghe, and H. Hallez, "Influence of Skull Modeling Approaches on EEG Source Localization," *Brain Topogr.*, vol. 27, no. 1, pp. 95–111, Jan. 2014.

[20] L. D. J. Fiederer *et al.*, "The role of blood vessels in high-resolution volume conductor head modeling of EEG," *Neuroimage*, vol. 128, pp. 193–208, 2016.

[21] L. Horesh, "Some Novel Approaches in Modelling and Image Reconstruction for Multi-Frequency Electrical Impedance Tomography of the Human Brain," University College London, 2006.

[22] X. Li, K. Yu, and B. He, "Magnetoacoustic tomography with magnetic induction (MAT-MI) for imaging electrical conductivity of biological tissue: a tutorial review," *Phys. Med. Biol.*, vol. 61, no. 18, pp. R249–R270, Sep. 2016.

[23] N. Gao, S. A. Zhu, and B. He, "A new magnetic resonance electrical impedance tomography (MREIT) algorithm: the RSM-MREIT algorithm with applications to estimation of human head conductivity," *Phys. Med. Biol.*, vol. 51, no. 12, pp. 3067–3083, Jun. 2006.

[24] Xiaotong Zhang, Dandan Yan, Shanan Zhu, and Bin He, "Noninvasive Imaging of Head-Brain Conductivity Profiles," *IEEE Eng. Med. Biol. Mag.*, vol. 27, no. 5, pp. 78–83, Sep. 2008.

[25] E. J. Woo and J. K. Seo, "Magnetic resonance electrical impedance tomography (MREIT) for high-resolution conductivity imaging," *Physiol. Meas.*, vol. 29, no. 10, pp. R1–R26, Oct. 2008.

[26] Xiaotong Zhang, Jiaen Liu, and Bin He, "Magnetic-Resonance-Based Electrical Properties Tomography: A Review," *IEEE Rev. Biomed. Eng.*, vol. 7, pp. 87–96, 2014.

[27] D. Gutierrez, A. Nehorai, and C. H. Muravchik, "Estimating Brain Conductivities and Dipole Source Signals With EEG Arrays," *IEEE Trans. Biomed. Eng.*, vol. 51, no. 12, pp. 2113–2122, Dec. 2004.

[28] Z. Akalin Acar, C. E. Acar, and S. Makeig, "Simultaneous head tissue conductivity and EEG source location estimation," *Neuroimage*, vol. 124, pp. 168–180, Jan. 2016.

[29] M. Odabaee *et al.*, "Neonatal EEG at scalp is focal and implies high skull conductivity in realistic neonatal head models," *Neuroimage*, vol. 96, pp. 73–80, Aug. 2014.

[30] J. Dabek *et al.*, "Determination of head conductivity frequency response in vivo with optimized EIT-EEG," *Neuroimage*, vol. 127, pp. 484–495, Feb. 2016.

[31] R. H. Bayford, "BIOIMPEDANCE TOMOGRAPHY (ELECTRICAL IMPEDANCE TOMOGRAPHY)," *Annu. Rev. Biomed. Eng.*, vol. 8, no. 1, pp. 63–91, Aug. 2006.

[32] David S. Holder, *Electrical Impedance Tomography: Methods, History and Applications (Series in Medical Physics and Biomedical Engineering)*. Institute of Physics, 2005.

[33] K. J. Eriksen, "In vivo human head regional conductivity estimation using a three-sphere model," in *Proc. of the Annual Conf. on Engineering in Medicine and Biology*, 1990, pp. 1494–1495.

[34] S. I. Turovets, P. Poolman, A. Salman, A. D. Malony, and D. M. Tucker, "Conductivity Analysis for High-Resolution EEG," *2008 Int. Conf. Biomed. Eng. Informatics*, vol. c, pp. 386–393, May 2008.

[35] M. Fernández-Corazza *et al.*, "Analysis of parametric estimation of head tissue conductivities using Electrical Impedance Tomography," *Biomed Signal Proces*, vol. 8, no. 6, pp. 830–837, 2013.

[36] D. S. Tuch, V. J. Wedeen, A. M. Dale, J. S. George, and J. W. Belliveau, "Conductivity Tensor Mapping of the Human Brain Using Diffusion Tensor MRI," *Proc Natl Acad Sci U S A*, vol. 98, no. 20, pp. 11697–11701, 2001.

[37] S. B. Baumann, D. R. Wozny, S. K. Kelly, and F. M. Meno, "The electrical conductivity of human cerebrospinal fluid at body temperature," *IEEE Trans. Biomed. Eng.*, vol. 44, no. 3, pp. 220–223, 1997.

[38] S. Rush and D. a Driscoll, "Current distribution in the brain from surface electrodes," *Anesth Analg*, vol. 47, no. 6, pp. 717–723, 1968.

[39] E. Frank, "Electric Potential Produced by Two Point Current Sources in a Homogeneous Conducting Sphere," *J. Appl. Phys.*, vol. 23, no. 11, pp. 1225–1228, 1952.

[40] J. D. Jackson, *Classical Electrodynamics Second Edition*. New York: John Wiley & Sons, 1975.

[41] J. C. de Munck and M. J. Peters, "A fast method to compute the potential in the multisphere model," *IEEE Trans. Biomed. Eng.*, vol. 40, no. 11, pp. 1166–1174, 1993.

[42] M. Fernández-Corazza, N. von-Ellenrieder, and C. H. Muravchik, "Estimation of electrical conductivity of a layered spherical head model using electrical impedance tomography," *J Phys Conf Ser*, vol. 332, no. 1, 2011.

[43] Z. Xu, W. He, C. He, Z. Zhang, and Z. Liu, "The Analytical Solution of EIT Forward Problem Based on A Multilayer Spherical Model," no. 2006.

[44] S. Turovets, V. Volkov, A. Zherdetsky, A. Prakonina, and A. D. Malony, "A 3D Finite-Difference BiCG Iterative Solver with the Fourier-Jacobi Preconditioner for the Anisotropic EIT/EEG Forward Problem," *Comput. Math. Methods Med.*, vol. 2014, pp. 1–12, 2014.

[45] A. Salman, S. Turovets, A. Malony, J. Eriksen, and D. Tucker, "Computational modeling of human head conductivity," in *Lecture Notes in Computer Science*, 2005, I., vol. 3514, pp. 631–638.

[46] U. Baysal and B. M. Eyüboglu, "Use of a priori information in estimating tissue resistivities - a simulation study," *Phys. Med. Biol.*, vol. 43, no. 12, pp. 3589–3606, Dec. 1998.

[47] A. Salman, A. Malony, S. Turovets, and D. Tucker, "Use of Parallel Simulated Annealing for Computational Modeling of Human Head Conductivity," 2007, pp. 86–93.

[48] T. de C. Martins, M. de S. G. Tsuzuki, E. D. L. B. de Camargo, R. G. Lima, F. S. de Moura, and M. B. P. Amato, "Interval Simulated Annealing applied to Electrical Impedance Tomography image reconstruction with fast objective function evaluation," *Comput. Math. with Appl.*, vol. 72, no. 5, pp. 1230–1243, Sep. 2016.

[49] H. C. Burger and J. B. Milaan, "Measurements of the specific Resistance of the human Body to direct Current," *Acta Med. Scand.*, vol. 114, no. 6, pp. 584–607, Apr. 1943.

[50] J. C. De Munck, T. J. C. Faes, A. J. Hermans, and R. M. Heethaar, "A Parametric Method to Resolve the Ill-Posed Nature of the EIT Reconstruction Problem: A Simulation Study," *Ann. N. Y. Acad. Sci.*, vol. 873, no. 1 ELECTRICAL BI, pp. 440–453, Apr. 1999.

[51] T. F. F. Oostendorp, J. Delbeke, and D. F. F. Stegeman, "The conductivity of the human skull: results of in vivo and in vitro measurements," *IEEE Trans. Biomed. Eng.*, vol. 47, no. 11, pp. 1487–1492, 2000.

[52] Y. Lai *et al.*, "Estimation of in vivo human brain-to-skull conductivity ratio from simultaneous extra- and intra-cranial electrical potential recordings," *Clin. Neurophysiol.*, vol. 116, no. 2, pp. 456–465, 2005.

[53] Y. Zhang, W. van Drongelen, M. Kohrman, and B. He, "Three-dimensional brain current source reconstruction from intra-cranial ECoG recordings," *Neuroimage*, vol. 42, no. 2, pp. 683–695, 2008.

[54] M. Clerc, G. Adde, J. Kybic, T. Papadopoulo, and J. Badier, "In vivo Conductivity Estimation with Symmetric Boundary Elements," *Int. J. Bioelectromagn.*, vol. 7, no. 1, pp. 307–310, 2005.

[55] Y. Zhang, W. Van Drongelen, and B. He, "Estimation of in vivo brain-to-skull conductivity ratio in humans," *Appl Phys Lett*, vol. 89, no. 22, pp. 22–25, 2006.

[56] T. Ouypornkochagorn, N. Polydorides, and H. McCann, "In Vivo Estimation of the Scalp and Skull Conductivity," in *15th Int. Conf. on Biomed. App. of Electrical Impedance Tomography*, 2014, p. 10.

[57] L. a Geddes and L. E. Baker, "The specific resistance of biological material-A compendium of data for the biomedical engineer and physiologist," *Med. Biol. Eng.*, vol. 5, no. 3, pp. 271–293, 1967.

[58] R. Hoekema *et al.*, "Measurement of the conductivity of skull, temporarily removed during epilepsy surgery," *Brain Topogr.*, vol. 16, no. 1, pp. 29–38, 2003.

[59] S. K. Law, "Thickness and resistivity variations over the upper surface of the human skull," *Brain Topogr.*, vol. 6, no. 2, pp. 99–109, Dec. 1993.

[60] M. Fernandez-Corazza, S. Turovets, P. Govyadinov, C. H. Muravchik, and D. Tucker, "Effects of Head Model Inaccuracies on Regional Scalp and Skull Conductivity Estimation Using Real EIT Measurements," in *IFMBE Proceedings: II Latin American Conference on Bioimpedance*,

2016, vol. 54, pp. 4–7.

[61] K. Li, X. Papademetris, and D. M. Tucker, "BrainK for Structural Image Processing: Creating Electrical Models of the Human Head," *Comput. Intell. Neurosci.*, vol. 2016, pp. 1–25, 2016.

[62] G. S. Russell, K. Jeffrey Eriksen, P. Poolman, P. Luu, and D. M. Tucker, "Geodesic photogrammetry for localizing sensor positions in dense-array EEG," *Clin. Neurophysiol.*, vol. 116, no. 5, pp. 1130–1140, May 2005.

[63] J. Song *et al.*, "Anatomically Accurate Head Models and Their Derivatives for Dense Array EEG Source Localization," *Funct Neurol Rehabil Erg.*, vol. 3, no. 2--3, pp. 275–293, 2013.

[64] P. Govyadinov, A. Gunn, S. Turovets, D. Tucker, and P. Luu, "Iontophoretic conditioning of the electrode to skin contacts," in *15th Int. Conf. on Biomed. App. of Electrical Impedance Tomography*, p. 36.

[65] B. Esler, T. Lyons, S. Turovets, and D. Tucker, "Instrumentation for low frequency EIT studies of the human head and its validation in phantom experiments," *J. Phys. Conf. Ser.*, vol. 224, no. 1, p. 12007, Apr. 2010.

[66] P. Poolman, R. M. Frank, and S. I. Turovets, "Modified Lock-In Detection for Extraction of Impressed EEG Signals in Low-Frequency Bounded-EIT Studies of the Human Head," in *2008 Congress on Image and Signal Processing*, 2008, vol. 1, pp. 174–183.

[67] Q. Fang and D. A. Boas, "Tetrahedral Mesh Generation from Volumetric Binary and Gray-scale Images," in *Proceedings of the Sixth IEEE International Conference on Symposium on Biomedical Imaging: From Nano to Macro*, 2009, pp. 1142–1145.

[68] A. Tizzard, L. Horesh, R. J. Yerworth, D. S. Holder, and R. H. Bayford, "Generating accurate finite element meshes for the forward model of the human head in EIT," *Physiol. Meas.*, vol. 26, no. 2, pp. S251–S261, Apr. 2005.

[69] The CGAL Project, *CGAL User and Reference Manual*, 4.9. CGAL Editorial Board, 2016.

[70] H. Si, "TetGen, a Delaunay-Based Quality Tetrahedral Mesh Generator," *ACM Trans. Math. Softw.*, vol. 41, no. 2, pp. 1–36, Feb. 2015.

[71] C. Gabriel, S. Gabriel, and E. Corthout, "The dielectric properties of biological tissues: I. Literature survey.," *Phys. Med. Biol.*, vol. 41, no. 11, pp. 2231–49, Nov. 1996.

[72] S. Gabriel, R. W. Lau, and C. Gabriel, "The dielectric properties of biological tissues: II. Measurements in the frequency range 10 Hz to 20 GHz.," *Phys. Med. Biol.*, vol. 41, no. 11, pp. 2251–69, Nov. 1996.

[73] G. Lindenblatt and J. Silny, "A model of the electrical volume conductor in the region of the eye in the ELF range.," *Phys. Med. Biol.*, vol. 46, no. 11, pp. 3051–9, Nov. 2001.

[74] P. Minhas *et al.*, "Electrodes for high-definition transcutaneous DC stimulation for applications in drug delivery and electrotherapy, including tDCS," *J. Neurosci. Methods*, vol. 190, no. 2, pp. 188–197, Jul. 2010.

[75] J. Malmivuo and R. Plonsey, *Bioelectromagnetism: Principles and Applications of Bioelectric and Biomagnetic Fields*. Oxford University Press, 1995.

[76] W. Lionheart, N. Polydorides, and A. Borsic, "The Reconstruction Problem," *Electr. Impedance Tomogr. Methods, Hist. Appl.*, vol. 32, no. December 2004, pp. 3–64, Aug. 2004.

[77] Y. W. Kwon and H. Bang, *The Finite Element Method Using MATLAB (2Nd Ed.)*. Boca Raton, FL, USA: CRC Press, Inc., 2000.

[78] P. P. Silvester and R. L. Ferrari, *Finite Elements for Electrical Engineers*. Cambridge: Cambridge University Press, 1994.

[79] R. Barrett *et al.*, *Templates for the Solution of Linear Systems: Building Blocks for Iterative Methods, 2nd Edition*. Philadelphia, PA: SIAM, 1994.

[80] S. M. Kay, *Fundamentals of statistical signal processing: estimation theory*. Upper Saddle River, NJ, USA: Prentice-Hall, Inc., 1993.

[81] M. . van Burik and M. . Peters, "Estimation of the electric conductivity from scalp measurements: feasibility and application to source localization," *Clin. Neurophysiol.*, vol. 111, no. 8, pp. 1514–1521, Aug. 2000.

[82] E. M. Essaki Arumugam, S. Turovets, N. Price, D. Rech, P. Luu, and D. M. Tucker, "In-vivo estimation of scalp and skull conductivity using bEIT for non-invasive neuroimaging and stimulation.," in *Brain Stimulation and Imaging Meeting*, 2017.

[83] J. C. Lagarias, J. A. Reeds, M. H. Wright, and P. E. Wright, "Convergence Properties of the Nelder--Mead Simplex Method in Low Dimensions," *SIAM J. Optim.*, vol. 9, no. 1, pp. 112–147, Jan. 1998.

[84] M. Akhtari *et al.*, "A model for frequency dependence of conductivities of the live human skull," *Brain Topogr.*, vol. 16, no. 1, pp. 39–55, 2003.

[85] A. Salman, A. Malony, S. Turovets, V. Volkov, O. D, and D. M. Tucker, "Concurrency in Electrical Neuroinformatics: Parallel Computation for Studying the Volume Conduction of Brain Electrical Fields in Human Head Tissues," *Concurr. Comput. Pr. Exper*, 2015.

[86] J. Song *et al.*, "EEG source localization: Sensor density and head surface coverage," *J. Neurosci. Methods*, vol. 256, pp. 9–21, Dec. 2015.

[87] R. D. Pascual-Marqui, "Standardized low-resolution brain electromagnetic tomography (sLORETA): technical details.," *Methods Find. Exp. Clin. Pharmacol.*, vol. 24 Suppl D, no. SUPPL. D, pp. 5–12, 2002.

[88] Z. A. Acar and S. Makeig, "Neuroelectromagnetic Forward Head Modeling Toolbox," *J. Neurosci. Methods*, vol. 190, no. 2, pp. 258–270, Jul. 2010.

[89] F. Tadel, S. Baillet, J. C. Mosher, D. Pantazis, and R. M. Leahy, "Brainstorm: A User-Friendly Application for MEG/EEG Analysis," *Comput. Intell. Neurosci.*, vol. 2011, pp. 1–13, 2011.

[90] R. Oostenveld, P. Fries, E. Maris, and J.-M. Schoffelen, "FieldTrip: Open Source Software for Advanced Analysis of MEG, EEG, and Invasive Electrophysiological Data," *Comput. Intell. Neurosci.*, vol. 2011, pp. 1–9, 2011.

[91] Y.-J. Jung, J.-H. Kim, and C.-H. Im, "COMETS: A MATLAB toolbox for simulating local electric fields generated by transcranial direct current stimulation (tDCS)," *Biomed. Eng. Lett.*, vol. 3, no. 1, pp. 39–46, Mar. 2013.

[92] M. Dannhauer, D. Brooks, D. Tucker, and R. MacLeod, "A pipeline for the simulation of transcranial direct current stimulation for realistic human head models using SCIRun/BioMesh3D," in *2012 Annual International Conference of the IEEE Engineering in Medicine and Biology Society*, 2012, pp. 5486–5489.

[93] C. Tang *et al.*, "Correlation between structure and resistivity variations of the live human skull," *IEEE Trans. Biomed. Eng.*, vol. 55, no. 9, pp. 2286–2292, 2008.

[94] M. Akhtari *et al.*, "Conductivities of three-layer live human skull.," *Brain Topogr.*, vol. 14, no. 3, pp. 151–67, 2002.

[95] Ü. Aydin *et al.*, "Combining EEG and MEG for the Reconstruction of Epileptic Activity Using a Calibrated Realistic Volume Conductor Model," *PLoS One*, vol. 9, no. 3, p. e93154, Mar. 2014.

[96] P. C. Miranda, A. Mekonnen, R. Salvador, and P. J. Basser, "Predicting the electric field distribution in the brain for the treatment of glioblastoma," *Phys. Med. Biol.*, vol. 59, no. 15, pp. 4137–4147, Aug. 2014.

[97] H. Hallez *et al.*, "Review on solving the forward problem in EEG source analysis," *J. Neuroeng. Rehabil.*, vol. 4, no. 1, p. 46, 2007.

[98] S. P. Van Den Broek, F. Reinders, M. Donderwinkel, and M. J. Peters, "Volume conduction effects in EEG and MEG," *Electroencephalogr. Clin. Neurophysiol.*, vol. 106, no. 6, pp. 522–534, 1998.

[99] M. Dannhauer, B. Lanfer, C. H. Wolters, T. R. Knösche, and T. R. Kn??sche, "Modeling of the human skull in EEG source analysis," *Hum. Brain Mapp.*, vol. 32, no. 9, pp. 1383–1399, 2011.

[100] D. Q. Truong, G. Magerowski, G. L. Blackburn, M. Bikson, and M. Alonso-Alonso, "Computational modeling of transcranial direct current stimulation (tDCS) in obesity: Impact of head fat and dose guidelines," *NeuroImage Clin.*, vol. 2, pp. 759–766, 2013.

[101] C. Schmidt, S. Wagner, M. Burger, U. van Rienen, and C. H. Wolters, "Impact of uncertain head tissue conductivity in the optimization of transcranial direct current stimulation for an auditory target," *J. Neural Eng.*, vol. 12, no. 4, p. 46028, Aug. 2015.

[102] C. Wenger, R. Salvador, and P. J. Basser, "The electric field distribution in the brain during TTFields therapy and its dependence on tissue dielectric properties and anatomy : a computational study," *Phys. Med. Biol.*, vol. 7339, p. 7339.

[103] L. Santos *et al.*, "Evaluation of the electric field in the brain during transcranial direct current stimulation: A sensitivity analysis," in *2016 38th Annual International Conference of the IEEE Engineering in Medicine and Biology Society (EMBC)*, 2016, pp. 1778–1781.

[104] S. Babaeizadeh, D. H. Brooks, D. Isaacson, and J. C. Newell, "Electrode boundary conditions and experimental validation for BEM-based EIT forward and inverse solutions," *IEEE Trans. Med. Imaging*, vol. 25, no. 9, pp. 1180–1188, Sep. 2006.

[105] C. Ramon, P. Garguilo, E. A. Fridgeirsson, and J. Haueisen, "Changes in scalp potentials and spatial smoothing effects of inclusion of dura layer in human head models for EEG simulations," *Front. Neuroeng.*, vol. 7, Aug. 2014.

This article has been accepted for publication in a future issue of this journal, but has not been fully edited. Content may change prior to final publication. Citation information: DOI 10.1109/TBME.2017.2777143, IEEE Transactions on Biomedical Engineering

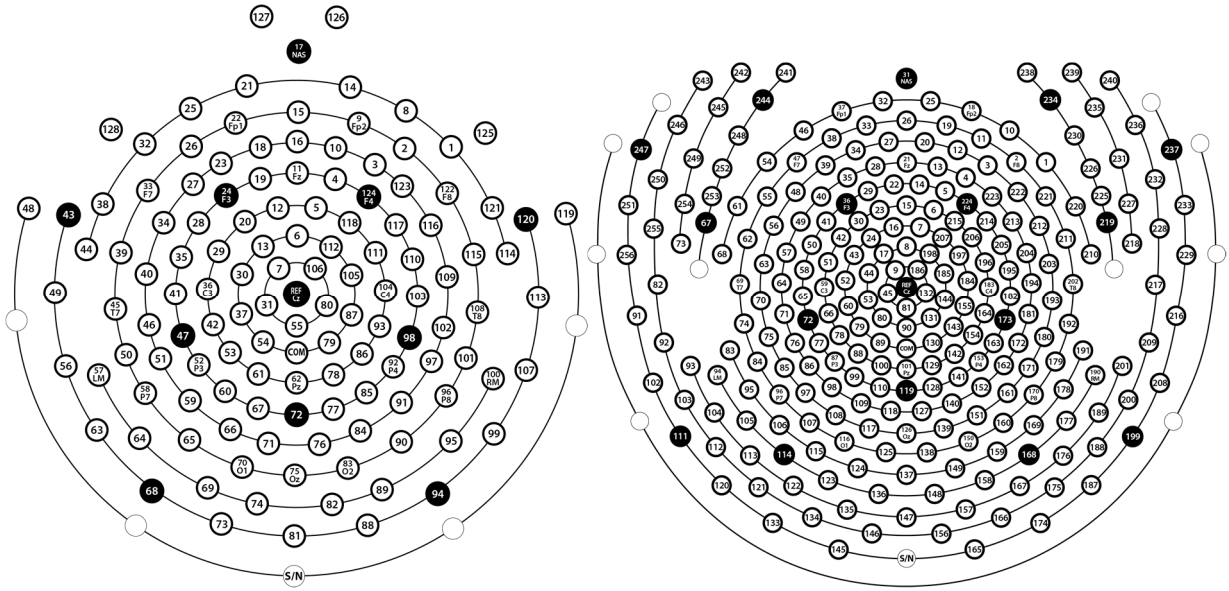

Fig S1: EGI 128 (left) and 256 (right) sensor net layouts.

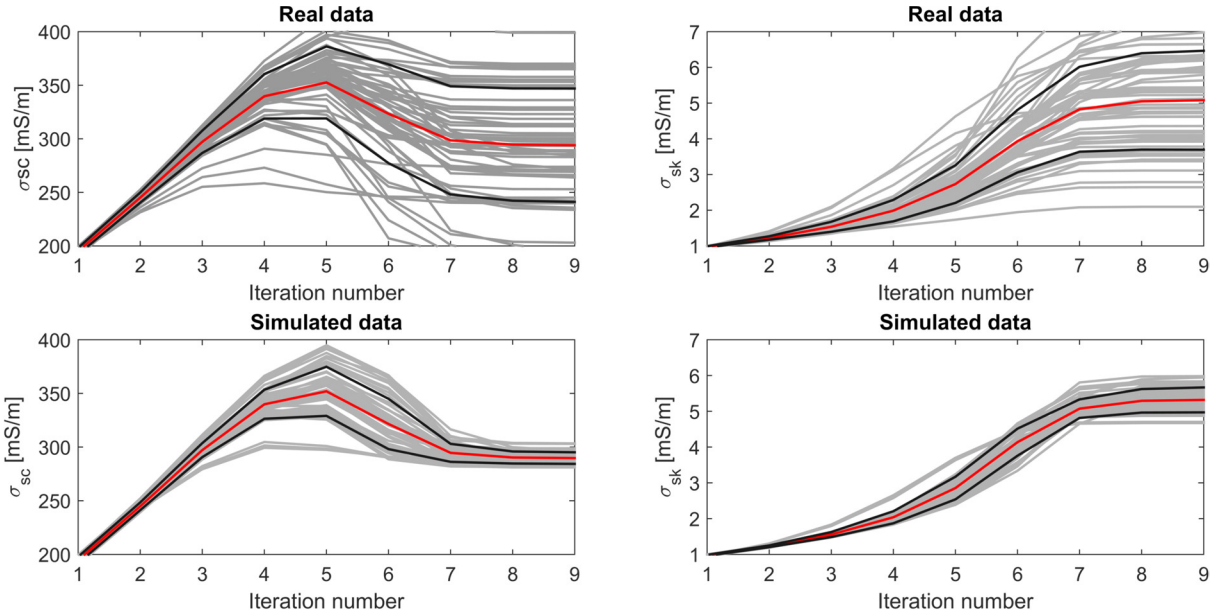

Fig S2: Convergence of the Newton's method for the scalp (left column) and the skull (right column) conductivity values for CA subject. In each figure subplot, we show an example of how the method converges after 9 iterations for both the real and synthetic data. The synthetic data was generated using the HQ model, and the conductivity values were estimated using the "HQ without marrow" model (2-parameter search). Each gray line represents a different current injection pair, the red line is the mean and the black lines represent the standard deviation.